The microstructure of mandibular bone grafts and three-dimensional cell clusters

Sarper Gürel[a], Corinne Unold[a,b], Hans Deyhle[a,b], Georg Schulz[a], Sebastian Kühl[b], Belma Saldamli[c], Jutta Tübel[c], Rainer Burgkart[c], Felix Beckmann[d], and Bert Müller[a,b,*]

[a]Biomaterials Science Center, University of Basel, 4031 Basel, Switzerland;
[b]School of Dental Medicine, University of Basel, 4056 Basel, Switzerland;
[c]Department of Orthopedic Surgery, Klinikum r. d. Isar, TU München, 81675 Munich, Germany;
[d]GKSS-Research Center, 21502 Geesthacht, Germany

ABSTRACT

During the last decade, several tissues and biomaterials for medical applications in replacing bony tissues have been developed. Three-dimensional cell clusters and mandibular bone grafts are two distinct examples of these developments. The characterization of the complex three-dimensional structures, however, is still mainly restricted on the two-dimensional analysis of histological slices. The present paper examines the quantitative analysis of mandibular bone grafts and three-dimensional cell clusters on the basis of synchrotron radiation-based micro computed tomography measurements. An automated search of pre-defined microstructures through component labeling is applied to the real datasets in order to identify features that reside independently from other components. The examples demonstrate three levels of complexity: rather large pieces of bone augmentation material that touch each other, individual adipocytes difficult to automatically segment in a wet cluster and osmium-stained adipocyte exhibiting higher X-ray absorption than the surrounding tissue. Although the structures of interest such as the cells can be labeled, de-clustering of the components requires the incorporation of erosion and dilation algorithms.

Keywords: three-dimensional cell cluster, bone graft, socket preservation, synchrotron radiation, micro computed tomography, component labeling, adipocyte

1. INTRODUCTION

Medically relevant man-made materials as well as biological tissues are generally anisotropic and inhomogeneous down to the nanometer scale [1]. Therefore, it is the dream of scientists and engineers to visualize the microstructures or even the nano-structures to understand the hierarchical morphology and the related function. Such an approach can also give feedback to optimize certain functionalities of human tissues especially for regenerative medicine. Consequently, the identification and labeling of components or individual microstructures is highly desirable. These algorithms are available, but have to be adapted to the real three-dimensional (3D) data, which are characterized by noise and artifacts. Furthermore, the algorithms are built on a variety of definitions, which can yield different quantities. For example, considering voxel-based tomography data, there are three definitions for connectivity. First, one can just count two objects as connected, if they have at least one touching face. For the cube, these are six possibilities. Second, if the two voxels have at least one edge together, the number of possibilities reaches 18. Third, if one adds common corners, the number rises to 26. It is still unclear, which of these definitions is the best choice for tomography data of biological tissues.

It has become more and more common to investigate the interface between implant material and the surrounding tissue not only by histological techniques but to include micro computed tomography (µCT) [2, 3]. The tomogram contains the full 3D information of implant and tissue, which allows for the extraction of the more or less complex interface [4]. The tomography data help the histologist to select the most interesting cutting positions. The more detailed histological data often provide additional insights into morphology but even more important on the functional states of the biosystem on cell level. In this way, histology and X-ray tomography are complementary techniques for the visualization of tissue morphology and function [5].

*bert.mueller@unibas.ch; phone +41 61 265 9660; fax +41 61 265 9699; www.bmc.unibas.ch

Bone augmentation using natural or artificial calcium phosphate phases is a common treatment before implant insertion, since the volume of bony tissue is often to small for implant insertion [6]. Because such a treatment needs months before the implant can be placed, it is highly desirable to identify the most effective biomaterials for bone augmentation. This can be easily done in following manner. The pre-defined set of patients gets comparable treatments using different ceramic biomaterials, which may differ in composition, feature size, and manufacturer. Before implant insertion, the oral surgeon prepares the hole for the implant by means of a hollow drill, which enables the scientists to store a representative specimen for detailed μCT measurements and analysis [7]. Finally, the acquired and reconstructed SRμCT data have to be evaluated with respect to bone density and architecture. The SRμCT data even allow analyzing the degradation of the ceramic biomaterial used for bone augmentation. Here, it is especially important to segment the biomaterial and bone components for quantification [4].

Most of the *in vitro* cell cultures rely on flat cell layers in petri dishes, although the human tissue is generally organized in 3D space. Therefore, developments in cell biology are directed to the growth on 3D scaffolds. Scaffolds, however, are the exception in human. Consequently, the development of scaffold-free culturing seems to be promising for many medical applications [8]. The quantitative evaluation of the fabricated histoids should support the understanding of cell cluster organization and the optimization of the culturing conditions.

Saldamli *et al.* [9] have shown by means of SRμCT that three-dimensional cell clusters contain spherically shaped features associated with the presence of adipocytes. The adipocyte is the most abundant stromal cell found in bone marrow. Similar to osteoblasts, adipocytes belong to the mesenchymal lineage and can differentiate from bone marrow stromal cells [10]. The presence of multiple refractive cytoplasmic droplets is an indicative morphological feature of adipocytes [11]. A positive staining of the droplets with lypochromes (dyes with lipid affinity such as osmium tetroxide) is confirmative for the phenotype of the cell.

Histologically, the mature adipocyte displays the typical signet-ring appearance, where a thin band of cytoplasm and the nucleus enclose a large, centrally located, lipid-laden vacuole. The immature adipocyte contains rather smaller and numerous lipid vacuoles [12]. However, during histological treatment lipid vacuoles in the cytoplasm may fuse. This is a well known phenomenon, related to prolonged/repeated ethanol exposure of adipocytes.

When isolated by collagenase digestion, adipocytes acquire a uniform spheroid shape [13]. The diameter of freshly isolated adipocytes from collagenase-treated human adipose tissue may range from about 22 to 120 μm, whereas the mean diameter may vary between 57 and 94 μm, depending on the employed measuring technique [14]. However, a population of very small fat cells of about 8 to 35 μm in diameter has been also described in some mammalian species [15].

The major function of the adipocyte is to store and release energy, therefore depending on the amount of lipid stored, its size can change up to several thousand fold [14]. Furthermore, adipocytes act as endocrine cells, secreting molecules that can regulate for example energy expenditure and glucose metabolism [16]. There is even some evidence that the size of the adipocyte is a major modulator of their endocrine function [17].

Studies on rodent and human marrow stromal populations have shown the existence of bi-potential progenitors, i.e. adipocyte-osteoblast precursor cells. There is abundant scientific evidence that plasticity exists between the osteogenic and adipogenic differentiation pathways and that these two lineages share a common multi-potent precursor [12, 18].

The present paper focuses on the quantitative analysis of microstructures for bone regeneration to finally improve patient treatments in dentistry and musculoskeletal degenerative diseases.

2. MATERIALS AND METHODS

2.1 Specimen preparation

A tooth of a 42-years old woman had to be extracted due to a longitudinal fracture. After tooth extraction under local anesthesia (Ultracain 4% DS 1:200.000, Aventis Pharma Deutschland GmbH, Frankfurt, Germany), the socket was filled with a well-established xenogenic bone substitute material (Bio-Oss®, Geistlich Biomaterials AG, Wolhusen, Switzerland). The socket was covered with a resorbable, double-layered collagen membrane (Bio-Guide®, Geistlich Biomaterials AG, Wolhusen, Switzerland) and single sutures were performed to fix the membrane *in situ*. One week later the sutures were removed. Five months after this grafting procedure, the patient presented for the insertion of a dental

implant into the grafted area. In order to gain a bony sample of the grafted material, a hollow bur by means of a dental trephine bur with an inner diameter of 3.2 mm was used for the preparation of the implant cavity. Such a bone graft specimen was gently removed from the trephine and immediately immersed in 4.5% buffered, pH 7.0 paraformaldehyde fixative (Roti Histofix 4.5%; Carl Roth GmbH + Co KG, Karlsruhe, Germany) for at least seven days. After de-hydrating in alcohol of increasing concentrations the sample was embedded into paraffin according to standard protocols (Hypercenter XP, Fa. Shandon, Frankfurt am Main, Germany) for histology.

For the histoids, human osteoblasts were isolated from femur neck cancellous bone and expanded in Dulbecco's Modified Eagle medium (Biochrom, Berlin, Germany) supplemented with 15% fetal calf serum (Biochrom, Berlin, Germany), 100 mg/l Primocin[TM] (InvivoGen, San Diego, CA, USA), 10 nM dexamethasone (Sigma, Steinheim, Germany), and 50 μg/ml ascorbic acid (Sigma, Steinheim, Germany). After confluence was reached, the cells proliferated further until multi-layer membranes with loose surface-contact were formed. Subsequently, the membranes were detached from the flask bottom to be collapsed in folded clusters. After a further seven days, the clusters were transferred into cell culture dishes to grow for at least 56 weeks. The details are given previously [9].

2.2 SRμCT-measurements

Bone graft, retrieved four months after socket preservation with a xenogenic (bovine) substitute material (Bio-Oss®, Geistlich Biomaterials AG, Wolhusen, Switzerland) was performed. For the acquisition at the GKSS-beamline W 2 (storage ring DORIS III at DESY, Hamburg, Germany) [20], the photon energy was set to 20 keV. 720 projections with an isotropic pixel size of 2.17 μm were taken between 0° and 180° with a spatial resolution of 3.23 mm determined by the 10%-value of the modulation transfer function of a highly X-ray absorbing metal edge [19]. The data were reconstructed with a filtered back-projection algorithm available at the beamline.

The tomograms of the histoids were acquired at the beamlines BW 2 (Histoid A) and W 2 (Histoid B) in absorption contrast mode. These experiments at the storage ring DORIS III (DESY, Hamburg, Germany) were operated by the GKSS-Research Center [20]. The photon energies were selected to 10 keV for Histoid A and 26 keV for Histoid B. The spatial resolution determined by the 10%-value of the modulation transfer function of a highly X-ray absorbing metal edge [19] was 6.8 μm at the isotropic pixel size of 5.2 μm and 4.2 μm at the pixel size of 2.6 μm, respectively. The tomograms were reconstructed by means of the standard filtered back-projection algorithm out of the 720 projections. For Histoid B the rotation axis of the specimen was asymmetric and the 1440 projections acquired from 0° to 360° were combined before reconstruction [21]. This approach is helpful to obtain high-resolution data from rather bulky specimens.

2.3 Data visualization

The 3D datasets of cell clusters and the mandibular bone grafts were visualized by means of the commercially available software VG Studio MAX 2.0 (Volume Graphics, Heidelberg, Germany).

2.4 Component labeling

Connected component labeling (CCL) is the process of identifying independent features in a dataset. In a connected component, it is possible to travel from one point to another by remaining inside the component boundaries. Such a structure can be visualized as a 3D island of immediately neighboring voxels. For 3D datasets, there are three types of connectivity definition, namely 6, 18, or 26. These types define the number of directions from which the neighboring voxels of the source voxel are checked, if they are a part of the same component. In this study, the 26-based connectivity is used for calculating the neighbors.

The procedure explained by the flow chart in Figure 1 is applied to the specimens in order to label the features detected. First, the local X-ray absorption values are plotted as histogram. The peaks were fitted by means of Gaussians to determine the X-ray absorption of the different materials with high precision and to select the thresholds for segmenting the microstructures of interest. The 3D data were low-pass filtered to reduce the noise improving segmentation and binarization. Subsequently, connected component labeling is applied. Initially, the number of features was huge, since the noise was only partially eliminated by the low-pass filter. Components smaller than a pre-defined value were filtered out. Finally, the components were labeled with a uniformly distributed random coloring, independent of their sizes and morphological properties. All data processing was performed with the MATLAB codes, version 7.8.0 (MathWorks, Natick, USA).
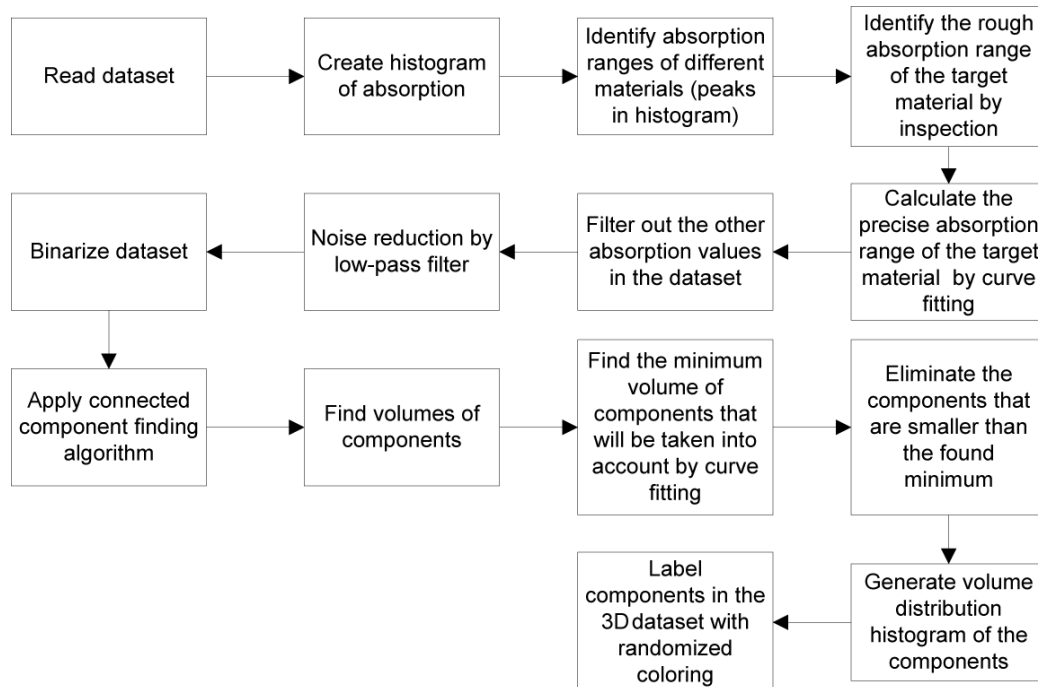
Figure 1. Flow chart explaining the steps for component labeling.

3. RESULTS

3.1 Bone graft

Tooth extraction is always associated with the resorption of the alveolar bone. Depending on the degree of resorption, alveolar reconstructions by means of grafting procedures can become necessary to form enough bone for secure implant insertion. Alveolar ridge- or socket preservation [22] is a grafting procedure that successfully reduces the resorption process. To achieve this, directly after tooth extraction, bone or bone substitute materials are inserted into the extraction site. The inserted material serves as a scaffold for the in-growth of blood vessels and bony tissues, whereby the success is defined as *osteoconduction*. Autogenous bone, in contrast to bone substitute materials, has additional *osteoinductive* properties, related to residual proteins and signaling molecules, which directly induce bone formation in the grafted area. The main disadvantage is the morbidity in the donor site and the limited amount, which makes bone substitute materials more practicable for grafting procedures. Though many studies evaluated the suitability of different grafting materials for socket preservation using histological sections retrieved several months after grafting procedure, which biomaterials are the most favorable ones is still a subject of discussion. Whenever dental implants are planed to rehabilitate the extraction site, it is desirable to obtain a maximum of formed bone, as only bone provides sufficient mechanical strength to resist to the forces that subsequently act on the implant and the surrounding tissue. Therefore, it is of clinical interest to gain knowledge on the 3D structure of the graft after healing into the socket.

The specimen extracted before implant insertion is visualized in Figure 2. The three orthogonal slices demonstrate that at least three species can be discriminated, i.e. the strongly X-ray absorbing graft material – bright, the bone formed (hard tissue) – gray and soft tissue – black like the surrounding air. The rather large differences in the local X-ray absorption usually allow for the easy extraction of the components of interest (see below).

The high-resolution X-ray tomography data show a wealth of details. The Bio-Oss® biomaterial exhibits sharp edges and a number of cracks, which might limit the performance of the biomaterial. In addition, one finds a high density of small pores and a few large pores assumed to be intentionally generated during preparation processes. It is quite interesting that similar pores are found in the bone formed. The bone is often in direct contact with the Bio-Oss®, which can be explained by its *osteoconductivity* properties. The size distribution of the different components (Bio-Oss®, bone, soft tissue) seems to be very similar, which is a prerequisite for optimized fatigue behavior. The medical expert would describe the biomaterial Bio-Oss® as appropriate for bone augmentation in the mandible.
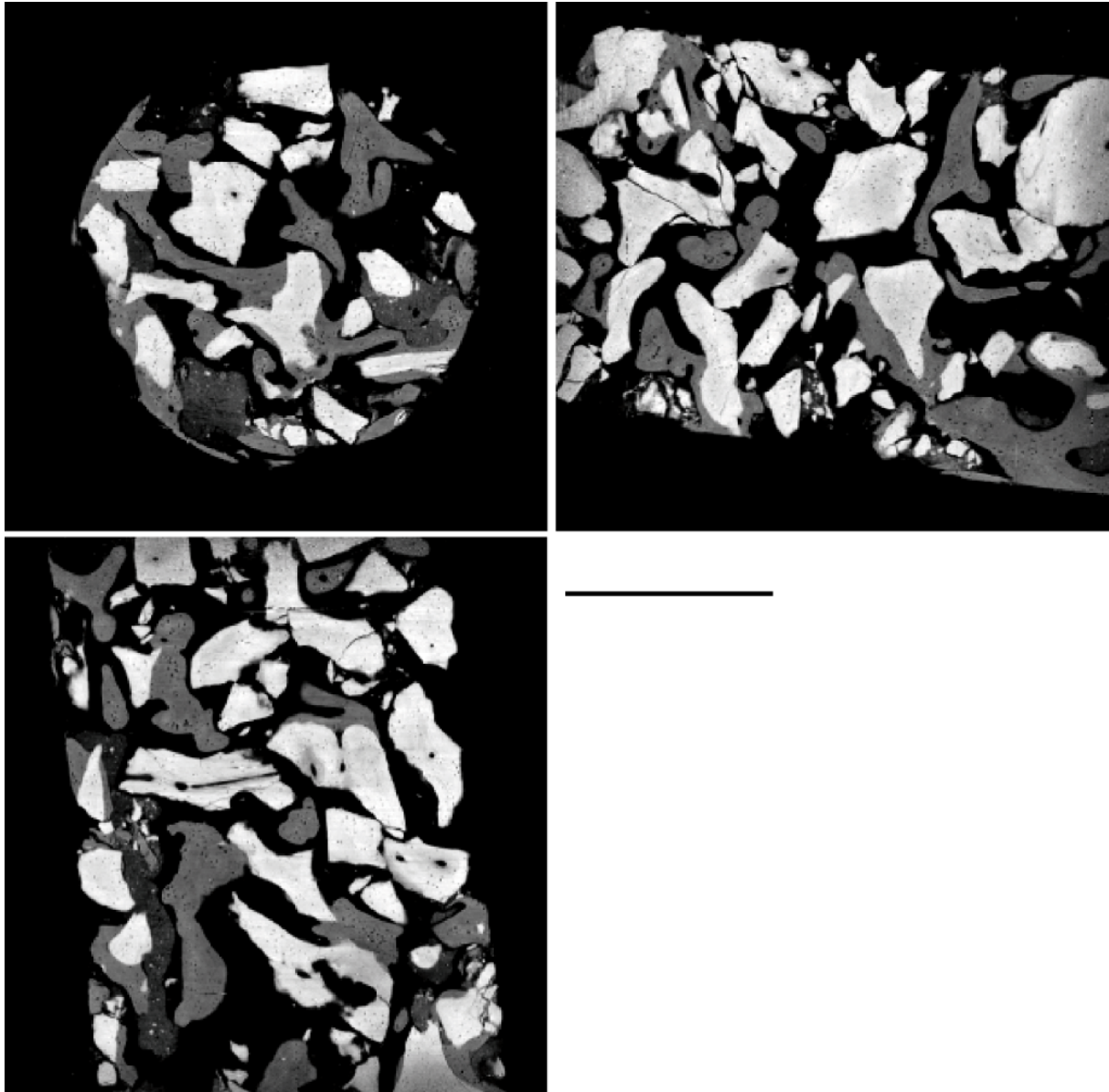
Figure 2. Three virtual orthogonal slices from the bone graft specimen after augmentation show the clear distinction of bone (gray) and bone graft (white). The spatial resolution is high enough to visualize pores in bone and graft. The scale bar corresponds to a length of 1 mm.

The SRμCT data, however, contain much more information, which can be used for a detailed analysis. Therefore, we evaluated the histogram of the local X-ray absorption values given in Figure 3. It allows discriminating not only between Bio-Oss® and bone, but reveals the presence of soft tissues, of the embedding material paraffin and the surrounding air.

The histogram is used to select an appropriate threshold for the intensity-based segmentation of the Bio-Oss®. At first, a Gaussian curve was fitted to the bone. The right flank of a second Gaussian was fitted to the biomaterial. In both cases, one obtains reasonable fitting. The mean X-ray absorption value of the two peak positions was selected to segment the bone graft material and to obtain a binarized 3D dataset. This dataset is the basis for the component labeling of the biomaterial particles in the specimen imaged by SRμCT.

For the quantitative evaluation of the microstructure and the mechanical stability, especially the fatigue behavior, the bone graft particles have to be identified and characterized according to shape, size, etc. Here, component labeling is an

established tool that allows identifying and numbering the objects of interest. Subsequently, these components can be listed and, for example, arranged according to size and shape. The 3D data also permit the evaluation of the spatial distribution.
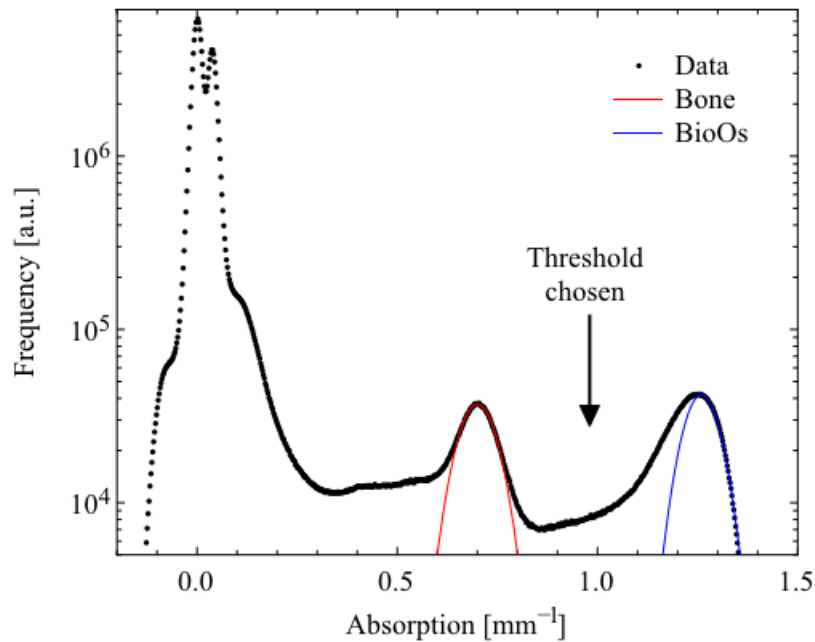

Figure 3. The absorption histogram of the specimen shown in Figure 2 permits discrimination between air, container/paraffin, soft tissues, hard tissues (bone) and the augmentation biomaterial (Bio-Oss®). Two Gaussians were fitted to the bone and Bio-Oss® peaks in order to select an appropriate threshold for the binarization of the bone graft material. The mean value of the peak positions has been chosen for the segmentation of the Bio-Oss®.

Figure 4 shows the result after the application of a MATLAB script based on the *bwconncomp* connected component labeling function included in the MATLAB image processing toolbox (version 7.8.0) to the specimen discussed above. The colors of components were selected by means of a uniformly distributed random generator, independent of the component size. One finds a dominating connected component, given in red. Here, one has the impression that many particles are combined maybe since they are rather close and noise leads to connection.

There are, however, further objects observed. Some of them appear to be just individual components as to be identified and there are others such as the blue-colored one, which seem to consist of many particles as the red-colored main component.

3.2 Three-dimensional cell cluster evaluation

Component labeling was applied to the data of Histoid A qualitatively presented by Saldamli *et al.* [9] in order to measure the diameter of the spherically shaped adipocytes. As a first step, the histogram of the X-ray absorption values that is represented in Figure 5 was extracted from the tomography data.

The histogram exhibits many peaks that can be associated with the surrounding air, the Eppendorf container, liquid around the cell cluster and the light protection layer on top of the container. The adipocytes exhibit an X-ray absorption, which does not result in an individual peak but just to an enhanced background-like signal. Therefore, the intensity-based segmentation is problematic. Nevertheless, one can segment the voxels having an X-ray absorption represented by the red-colored line, i.e. between about 0.3 and 0.4 mm^{-1}.
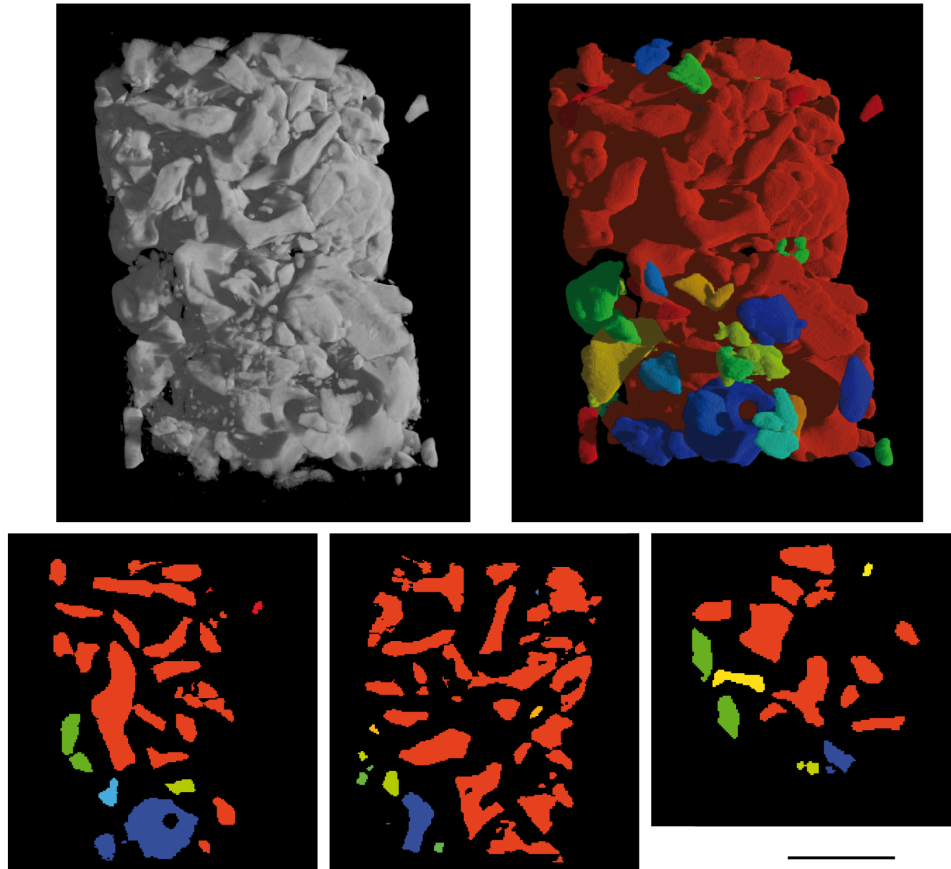
Figure 4. In the top line two 3D representations of the segmented bone graft biomaterial are given. While the left is a gray-scale image, the right one contains color-coded components. In the bottom line three selected slices orthogonally oriented to another of the color-labeled dataset are presented. The scale bar corresponds to 1 mm.
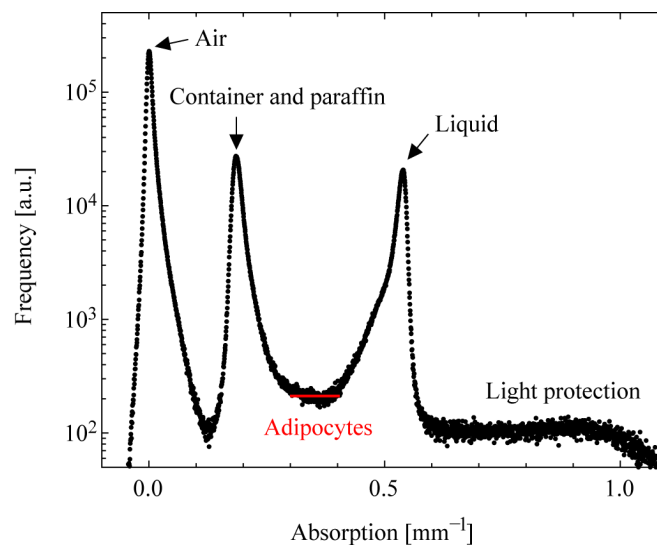

Figure 5. The X-ray absorption of adipocytes lies between the absorption peaks of container/paraffin and embedding liquid. From these data, one may conclude that the segmentation and labeling of the adipocytes is impossible.

The result of the component labeling is elucidated in Figure 6. On the left, a selected virtual cut through the entire dataset is given. One can see the gray-colored adipocytes, which also seem to form clusters. Because the stacked tomogram contains many artifacts such as X-ray-induced bubble formation, we have applied the component labeling to just a sub-volume, as shown by the box. Here, we also realized that many spherical units (adipocytes) form one component, as shown by the color codes. Consequently, the size of the spherically shaped cells cannot be automatically extracted.
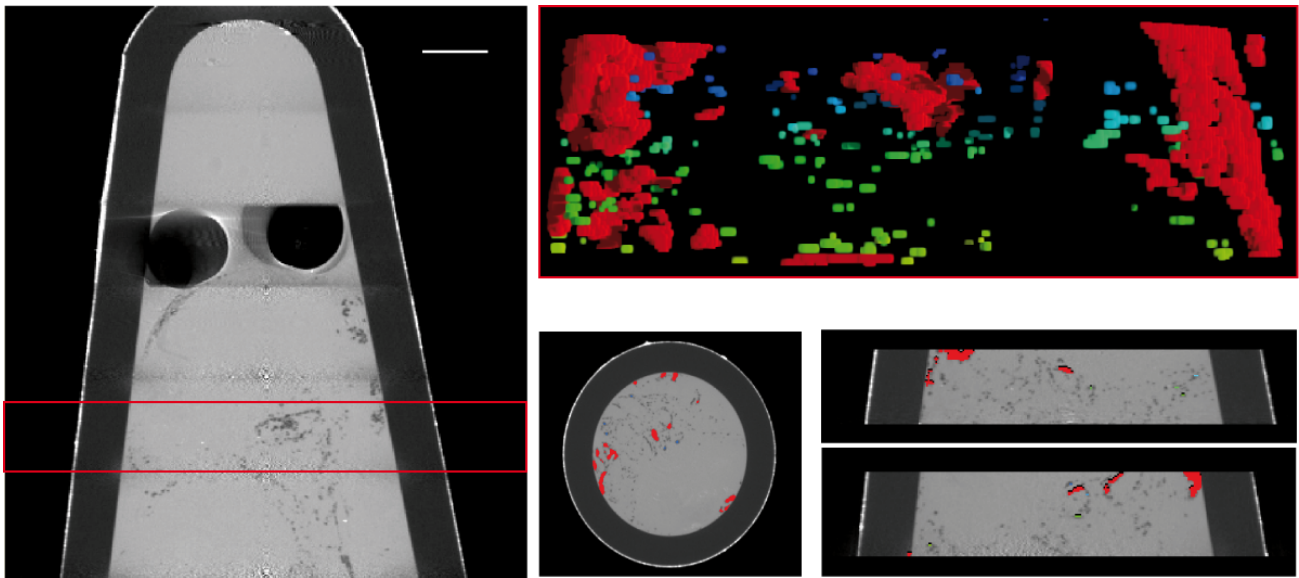

Figure 6. Component labeling is applied to a selected part of the stacked tomographic data, which has a relatively high concentration of adipocyte clusters. As seen best in the 3D view (top, right), bigger components are residing rather at the periphery of the cell cluster. On the 3 orthogonal slices (bottom, right), the bigger features are labeled, but many smaller features are present as easily observed by eye. The scale bar corresponds to 1 mm.

In order to improve the chances for labeling the adipocytes, a selective staining protocol was applied. Osmium is known to show a high affinity to bind to adipocytes. This behavior is verified by the histogram given in Figure 7, which was derived from SRμCT data of Histoid B. The osmium-stained adipocytes exhibit a much higher X-ray absorption than air, embedding and soft tissue components. Consequently, it is rather simple to segment the adipocytes by just considering the red-colored absorption range between about 0.65 and 1.3 mm^{-1} (see Figure 7). With other words, the X-ray absorption values of the cells are significantly shifted towards higher local absorption compared to the other less or non-stained parts of the specimen. The remaining problem is the broad shoulder to lower X-ray absorption values, which is predominately the result of partial volume phenomena. This is especially large, since the interface between the adipocytes and the surrounding is huge.

Figure 8 illustrates the component labeling of Histoid B. On the left, a conventional 3D representation of the gray-scale image is given, whereas on the right the related components are color-coded. In principle, the adipocytes were properly rendered. Nevertheless, the clustering of cells is still present and makes the quantification of the cell diameters difficult.

Based on the component labeling of Histoid B, the diameter of the spherically shaped adipocytes was determined. Although the datasets with a binning factor of two and three exhibit much better contrast [23], the spatial resolution was inappropriate for diameter quantification. Since the dataset of the entire specimen was huge, a region of interest with high cell density was selected. In order to remove the noise, the components smaller than 4 pixels length, i.e. less than 20 μm in diameter, were not considered for quantification. It should be mentioned that such small components cannot be classified as spherically shaped.

Observing the color-coded components in Figure 8, one finds many components consisting of cell clusters. These clusters are manually evaluated counting the number of cells within the individual clusters. As a result 662 adipocytes were identified. The largest adipocyte has a diameter of 66 μm. The mean cell diameter was found to be (41 ± 12) μm. The error bar is simply the standard deviation.
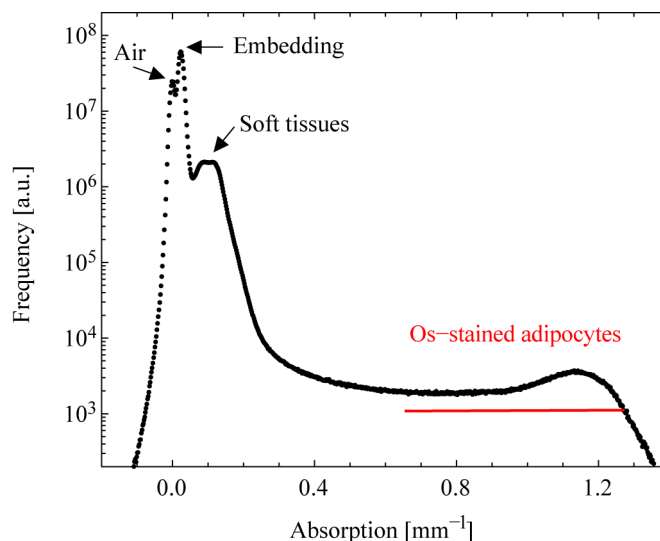
Figure 7. The absorption histogram of Os-stained adipocyte colonies shows a well-defined X-ray absorption range that is not overlapped by any other species.

4. DISCUSSION

Component labeling is often a prerequisite to evaluate the size, morphology, and size distribution of features within 3D data [24, 25]. The success of the algorithm has to be validated, which is frequently done manually. One critical issue is the choice of the threshold for intensity-based segmentation. If the peak maxima of the species to be segmented are of similar height, as in the example of the bone specimen after augmentation (cp. Figs. 2 and 3), the mean value is one of a few simple but reasonable possibilities. Nevertheless, many phenomena including partial volumes can massively influence the quantities extracted. Noise that is always present in X-ray tomography because of the limited photon statistics is another challenge and can result in clustered features as found in the two presented examples. There are, however, many noise-reducing procedures available, but these operations can also drastically modify the extracted quantities. The fragmentation of identified clusters into the individual units is often dangerous, especially if automated algorithms are applied. In the medical field, students frequently segment the features on 2D images in a manual fashion, which is laborious and could result in non-predictable errors. Certainly, independent analysis by different individuals can significantly reduce the failure rate, but also needs much higher efforts. More sophisticated algorithms, which are based on the visual inspection of the data, can help to simplify the data treatment and will lead to reliable quantities for the comparison of technical, biological, and medical processes.

The dedicated staining of the components of interest such as carried out for the adipocytes by osmium tetroxide is extremely supportive for the application of the automated algorithms. The staining, however, also modifies the specimen so that sizes of certain components become altered due to processes such as shrinkage. Nevertheless, the cell diameter of the adipocytes derived in the present study fits well to the data presented in the introduction. This is a valuable indication that the specimen preparation was suitable for quantifying the size and morphology of the adipocytes within the 3D cell culture.

5. CONCLUSION

Although component labeling is a well-established algorithm, its application to medically relevant high-resolution tomography data is not straightforward. One of the main issues is component clustering as seen here for a graft material and adipocytes. The fragmentation of the clusters into the individual units may be realized by means of suitable erosion and dilation steps based on sophisticated computer code and sound verification as already successfully applied to 3D cell cultures [23].
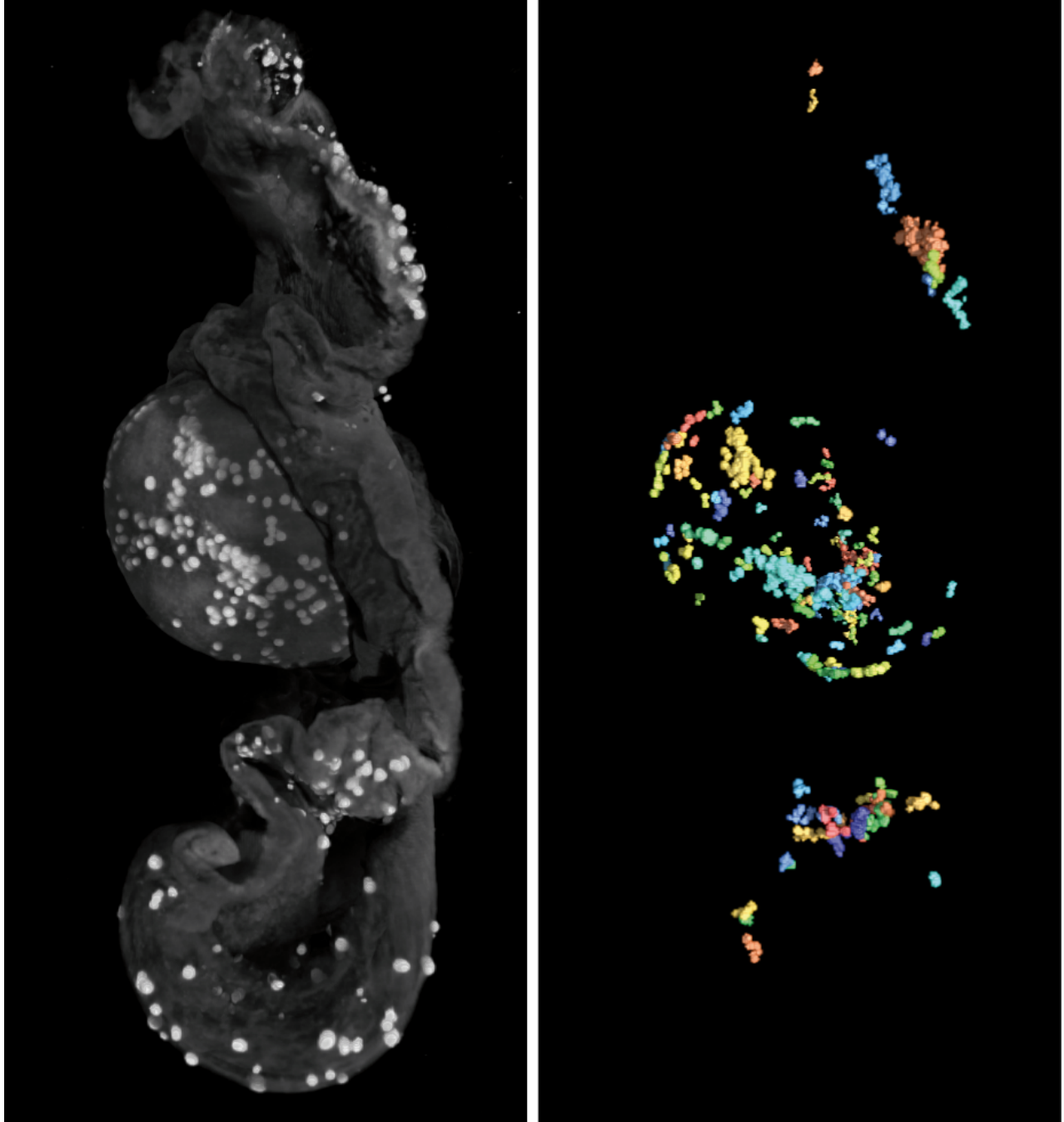
Figure 8. Three-dimensional representations of the gray-scale data (left) emphasizing the spherically shaped adipocytes and the related color-coded components (right) are given. Note that the adipocytes form clusters.

REFERENCES

[1] Müller, B., Deyhle, H., Bradley, D., Farquharson, M., Schulz, G., Müller-Gerbl, M., and Bunk, O., "Scanning X-ray scattering: Evaluating the nanostructure of human tissues," Eur. J. Clin. Nanomed. 3, 30-33 (2010).

[2] Chappard, D., Guillaume, B., Mallet, R., Pascaretti-Grizon, F., Baslé, M.F., and Libouban, H., "Sinus lift augmentation ant beta-TCP: a microCT and histological analysis on human bone biopsies," Micron 41(4), 321-326 (2010).

[3] Bernhardt, R., Scharnweber, D., Müller, B., Thurner, P., Schliephake, H., Wyss, P., Beckmann, F., Goebbels, J., and Worch, H., "Comparison of microfocus- and synchrotron X-ray tomography for the analysis of osteointegration around Ti6Al4V implants,", Eur. Cells Mater. 7, 42-51 (2004).

[4] Kuehl, S., Goetz, H., Hansen, T., Kreisler, M., Behneke, A., Heil, U., Duschner, H., and d Hoedt, B., "Three-dimensional analysis of bone formation after maxillary sinus augmentation by means of micro-computed tomography: A pilot study," Int. J. Oral Max. Surg., submitted (2010).

[5] Germann, M., Morel, A., Beckmann, F., Andronache, A., Jeanmonod, D., and Müller, B., "Strain fields in histological slices of brain tissue determined by synchrotron radiation-based micro computed tomography," J. Neurosci. Meth. 170, 149-155 (2008).

[6] Rabelo, G.D., de Paula, P.M., Rocha, F.S., Jordão Silva, C., and Zanetta-Barbosa, D., "Retrospective study of bone grafting procedures before implant placement," Implant Dent. 19(4), 342-350 (2010).

[7] Trisi, P., Rebaudi, A., Calvari, F., and Lazzara, R.J., "Sinusgraft with Biogran, autogenous bone, and PRP: A report of three cases with histology and micro-CT," Int. J. Periodont. Rest. 26(2), 113-125 (2006).

[8] Müller, B., Riedel, M., and Thurner, P., "Three-dimensional characterization of cell clusters using synchrotron-radiation-based micro computed tomography," Microsc. Microanal. 12, 97-105 (2006).

[9] Saldamli, B., Herzen, J., Beckmann, F., Tubel, J., Schauwecker, J., Burgkart, R., Jurgens, P., Zeilhofer, H.F., Sader, R., and Müller, B., "Internal structures of scaffold-free 3D cell cultures visualized by synchrotron radiation-based micro-computed tomography," Proc. SPIE 7078, 70781O (2008).

[10] Pittenger, M.F., Mackay, A.M., Beck, S.C., Jaiswal, R.K., Douglas, R., Mosca, J.D., Moorman, M.A., Simonetti, D.W., Craig, S., and Marshak, D.R., "Multilineage potential of adult human mesenchymal stem cells," Science 284(5411), 143-147 (1999).

[11] Laharrague, P., Larrouy, D., Fontanilles, A.M., Truel, N., Campfield, A., Tenenbaum, R., Galitzky, J., Corberand, J.X., Penicaud, L., and Casteilla, L., "High expression of leptin by human bone marrow adipocytes in primary culture," Faseb J. 12(9), 747-752 (1998).

[12] Gimble, J.M., Robinson, C.E., Wu, X., and Kelly, K.A., "The function of adipocytes in the bone marrow stroma: an update," Bone 19(5), 421-428 (1996).

[13] Chen, H.C. and Farese, R.V., Jr., "Determination of adipocyte size by computer image analysis," J. Lipid Res. 43(6), 986-989 (2002).

[14] Bjornheden, T., Jakubowicz, B., Levin, M., Oden, B., Eden, S., Sjostrom, L., and Lonn, M., "Computerized determination of adipocyte size," Obes. Res. 12(1), 95-105 (2004).

[15] DeMartinis, F.D. and Francendese, A., "Very small fat cell populations: mammalian occurrence and effect of age," J. Lipid Res. 23(8), 1107-1120 (1982).

[16] Spiegelman, B.M. and Flier, J.S., "Adipogenesis and obesity: rounding out the big picture," Cell 87(3), 377-389 (1996).

[17] Kubota, N., Terauchi, Y., Miki, H., Tamemoto, H., Yamauchi, T., Komeda, K., Satoh, S., Nakano, R., Ishii, C., Sugiyama, T., Eto, K., Tsubamoto, Y., Okuno, A., Murakami, K., Sekihara, H., Hasegawa, G., Naito, M., Toyoshima, Y., Tanaka, S., Shiota, K., Kitamura, T., Fujita, T., Ezaki, O., Aizawa, S., and Kadowaki, T., "PPAR gamma mediates high-fat diet-induced adipocyte hypertrophy and insulin resistance," Mol. Cell 4(4), 597-609 (1999).

[18] Park, S.R., Oreffo, R.O., and Triffitt, J.T., "Interconversion potential of cloned human marrow adipocytes in vitro," Bone 24(6), 549-554 (1999).

[19] Müller, B., Thurner, P., Beckmann, F., Weitkamp, T., Rau, C., Bernhardt, R., Karamuk, E., Eckert, L., Buchloh, S., Wintermantel, E., Scharnweber, D., and Worch, H., "Three-dimensional evaluation of biocompatible materials by microtomography using synchrotron radiation," Proc. SPIE 4503, 178-188 (2002).

[20] Beckmann, F., Herzen, J., Haibel, A., Müller, B., and Schreyer, A., "High density resolution in synchrotron-radiation-based attenuation-contrast microtomography," Proc. SPIE 7078, 70781D (2008).

[21] Müller, B., Bernhardt, R., Weitkamp, T., Beckmann, F., Bräuer, R., Schurigt, U., Schrott-Fischer, A., Glueckert, R., Ney, M., Beleites, T., Jolly, C., and Scharnweber, D., "Morphology of bony tissues and implants uncovered by high-resolution tomographic imaging," Int. J. Mater. Res. 98(7), 613-621 (2007).

[22] Maspero, F.A., Ruffieux, K., Müller, B., and Wintermantel, E., "Resorbable defect analog PLGA scaffolds using CO_2 as solvent: structural characterization," J. Biomed. Mater. Res. 61, 89-98 (2002).

[23] Thurner, P., Beckmann, F., and Müller, B., "An optimization procedure for spatial and density resolution in hard X-ray micro-computed tomography," Nucl. Instrum. Meth. B 225(4), 599-603 (2004).

[24] Chen, W.J., Giger, M.L., and Bick, U., "A fuzzy c-means (FCM)-based approach for computerized segmentation of breast lesions in dynamic contrast-enhanced MR images," Acad. Radiol. 13, 63-72 (2006).

[25] Yapa, R.D. and Koichi, H., "A connected component labeling algorithm for grayscale images and application of the algorithm on mammograms," Lecture Notes Computer Sci. 1/2, 146-152 (2007).